

Driven translocation of a semiflexible polymer through a conical channel in the presence of attractive surface interactions

Andri Sharma,^{*} Rajeev Kapri,[†] and Abhishek Chaudhuri[‡]

*Department of Physical Sciences, Indian Institute of Science Education and Research (IISER) Mohali,
Sector 81, S. A. S. Nagar 140306 Punjab, India*

(Dated: May 27, 2022)

We study the translocation of a semiflexible polymer through a conical channel with attractive surface interactions and a driving force which varies spatially inside the channel. Using the results of the translocation dynamics of a flexible polymer through an extended channel as control, we first show that the asymmetric shape of the channel gives rise to non-monotonic features in the total translocation time as a function of the apex angle of the channel. The waiting time distributions of individual monomer beads inside the channel show unique features strongly dependent on the driving force and the surface interactions. Polymer stiffness results in longer translocation times for all angles of the channel. Further, non-monotonic features in the translocation time as a function of the channel angle changes substantially as the polymer becomes stiffer, which is reflected in the changing features of the waiting time distributions. We construct a free energy description of the system incorporating entropic and energetic contributions in the low force regime to explain the simulation results.

I. INTRODUCTION

The translocation of macromolecules through nanopores and channels has been a topic of immense interest since the pioneering work by Kasianowicz et al. in which DNA was successfully translocated through a biological nanopore [1]. Study of confined polymers and translocation of polymers through geometrical pores paved a way to study sequencing of DNA and RNA, which has a lot of applications in the field of medicine and biotechnology. During the last few decades, a number of experimental and theoretical work has been performed to understand the dynamics of the transportation of such biomolecules [2–31].

The transport of DNA through a nanopore/nanochannel is facilitated by the application of an electric field across the channel, giving rise to an electrostatic force which pulls the DNA into the channel. Due to the reduction in conformational entropy of a polymer in confinement, the geometry of the nanochannel has been found to strongly affect the dynamics of the translocation process. For example, in DNA sequencing using biological nanopores like α -hemolysin and MspA, it has been observed that the shape of channel plays a vital role in determining the ionic current through it [32–39]. Compared to the α -hemolysin pore, where the cylindrical shape of the beta barrel dilutes the ion current specific to individual nucleotide of the DNA inside the channel, thus making sequencing difficult, the narrow constriction of the cone shaped MspA allows better resolution of current signatures corresponding to individual nucleotide [3, 40, 41].

In a bid to control the transport dynamics of the DNA inside the nanochannel to achieve better sequencing, experimental approaches have shifted to the building of bio-inspired nanopores and nanochannels with similar transport properties [42–46]. These artificial solid-state nanochannels not only allow the control of the shape of the channel and tunability of its surface properties, but are also stable with respect to changes in pH, temperature and mechanical oscillations. Asymmetrical conically shaped nanopores have been found to have excellent sensing applications, with the nanopore tip acting as a sensing zone [47–52]. Conical nanocapillaries show ionic current rectification at low salt concentrations. Further, chemical modifications of the inner surfaces of a conical nanochannel can lead to reversal in the ion current rectification direction. A combination of a conical nanofunnel with a cylindrical nanochannel, was shown to significantly reduce the threshold external voltage required to trigger the translocation of DNA through the channel [51].

Theoretical studies of polymer translocation through conical nanochannels have shown that the escape of a confined flexible polymer from a conical channel is a pore driven process and can proceed without an external force [53, 54]. The asymmetric shape of the channel ensures that the polymer has a larger entropic penalty near the constriction which gives rise to an entropic force leading to the escape of the polymer from the larger opening. Further, the passage time is a non-monotonic function of the apex angle of the cone for a given length of the channel. Langevin dynamics studies of flexible polymer translocation through conical channels have shown that translocation is dependent on channel structure and interactions of the polymer with the channel [34, 55, 56]. Most biopolymers and proteins are however semiflexible with an energy cost associated in bending, characterized by the bending rigidity κ of the polymer. It is with this motivation that we characterize the translocation dynam-

^{*} ph17007@iisermohali.ac.in

[†] rkapri@iisermohali.ac.in

[‡] abhishek@iisermohali.ac.in

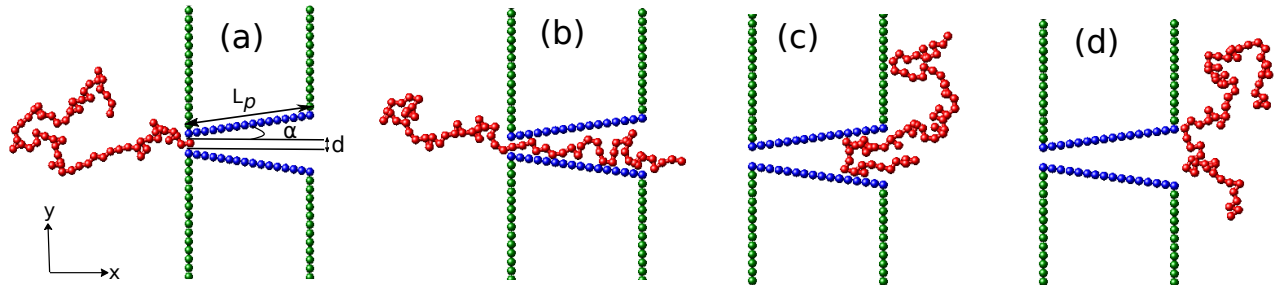


FIG. 1. Snapshots from the simulation for various stages of the translocation process of a semiflexible polymer with $N = 64$ beads, through a conical channel of length $L_p = 16\sigma$, half apex angle α and channel entrance width d . (a) Equilibrium polymer conformation on the *cis* side of the channel with one end fixed at the pore entrance. Subsequent polymer conformations (b) midway through the translocation process, (c) showing a possible hairpin formation near the channel exit and (d) when the polymer has successfully translocated to the *trans* side of the channel.

ics of a semiflexible polymer through an interactive conical nanochannel.

In this paper, we present a detailed study of translocation dynamics of both flexible and semiflexible polymers through cone shaped nanochannels in the presence of a spatially varying external driving force and surface interactions, using coarse-grained Langevin dynamics simulations. The external force acting along the channel length mimics the voltage driven translocation of polymers, higher at narrower regions of the channel and lower near the larger channel openings. We first report results of the waiting time distributions for a translocating flexible polymer for varying strengths of the external force for a fixed apex angle α of the channel (see Fig. 1(a)). The total translocation time τ decreases with increasing force strength as expected. With varying α , the translocation time shows non-monotonic features, consistent with earlier reports. We comment on the detailed behavior of the waiting time distribution with varying force strengths and α . We next present a detailed study of the translocation dynamics of semiflexible polymers with increasing stiffness through this conical nanochannel. The non-monotonic features observed in τ with varying α differs significantly from that of the flexible polymer. The translocation time is also strongly dependent on the stiffness of the polymer. Further, with increasing forces, the non-monotonic features reduce significantly and total translocation time increases with increasing α for all values of polymer stiffness. We present phase plots of τ in the $\kappa - \alpha$ plane and mean waiting time distributions to characterize the translocation dynamics in detail. Finally, we provide free energy arguments using a quasi-equilibrium approximation valid at low forces to explain our observations.

The paper is organized as follows. In section 2, we introduce the simulation model and methods where the governing equations are explained. This section also sets the notations used in the paper. In section 3, we present the results and discussion of our simulations for (a) flexible and (b) semiflexible polymer and provide possible explanation for the observed behaviour at low forces via

a free energy description. In section 4, we conclude by discussing the importance of our results and possible future directions to extend the domain of physical relevance of this work.

II. MODEL

To model the conical channel in two dimensions, we consider the walls of the channel to be made up of two rows of fixed monomer beads of size σ and of length $L_p = N'\sigma$, where N' is the number of monomers making up a wall of the channel. The walls are symmetric about the x -axis with the apex angle of the channel α defined with respect to the x -axis as shown in the Fig. 1. The diameter of the channel at the *cis* side is fixed at d to allow only single monomer entry. To separate the *cis* and *trans* regions of the channel, vertical walls made up of fixed monomers beads are placed along the y - direction.

The polymer is modeled via a coarse grained bead-spring chain, where non-bonded monomers interact via a short ranged repulsive Lennard-Jones (rLJ) potential given by

$$U_{\text{bead}}(r) = \begin{cases} 4\epsilon \left[\left(\frac{\sigma}{r}\right)^{12} - \left(\frac{\sigma}{r}\right)^6 \right] + \epsilon, & r < r_c \\ 0, & r \geq r_c \end{cases} \quad (1)$$

where ϵ gives the strength of the potential. The above truncated and shifted LJ potential has cut-off at $r_c = 2^{\frac{6}{5}}\sigma$. The interaction between consecutive monomers of the chain is harmonic with the interaction given by

$$U_{\text{bond}} = \frac{1}{2}K(r - r_0)^2, \quad (2)$$

where K is the spring constant and r_0 is the equilibrium separation between consecutive monomers.

To model a semiflexible polymer, an additional bending potential is introduced between consecutive bonds as

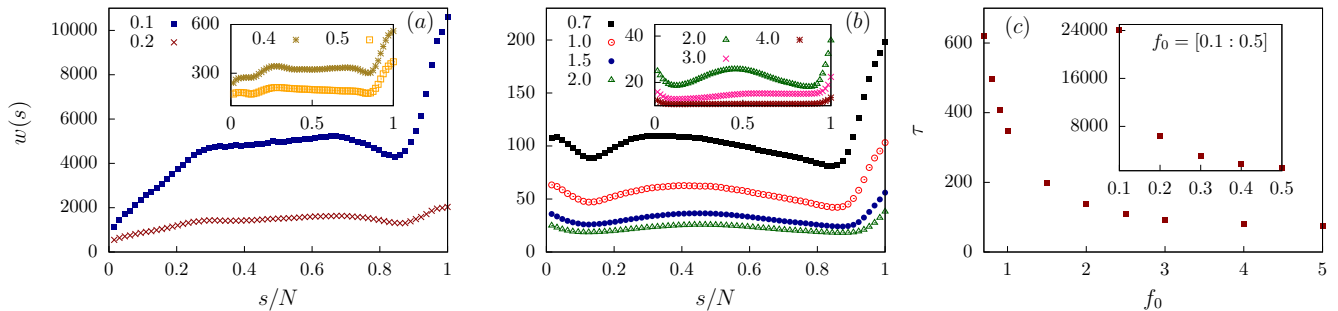


FIG. 2. (a) Waiting time distribution $w(s)$ of a flexible polymer through a flat channel ($\alpha = 0^\circ$) as a function of scaled translocation coordinate s/N , for weak forces : $f_0 = 0.1$ and $f_0 = 0.2$. (b) waiting time distribution for forces lying in the range $f_0 = [0.5 : 2.0]$. (Inset) $w(s)$ for even larger force values, $f_0 = 2.0, 3.0$ and 4.0 . (c) Total translocation time (τ) as a function of external force (f_0) showing a sharp decrease at larger force values. (Inset) Magnified plot of the same for lower force range.

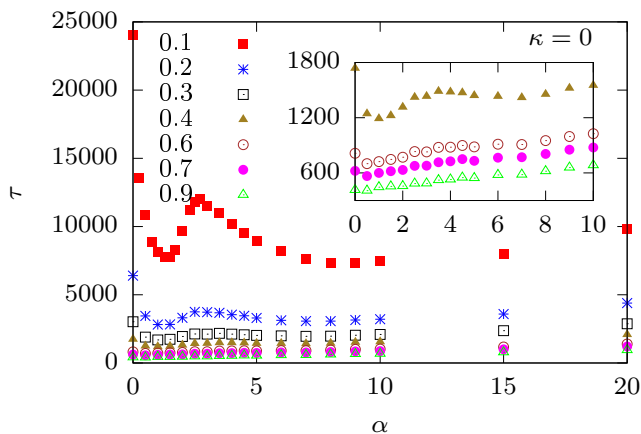


FIG. 3. Total translocation time (τ) of flexible polymer through attractive conical channel as a function of apex angle (α) for different external forces f_0 . (Inset) Magnified plot of τ versus α at larger force values showing the disappearance of maxima-minima peaks.

follows :

$$U_{\text{bend}}(\theta_i) = \kappa(1 + \cos \theta_i) \quad (3)$$

where θ_i is the angle between the i^{th} and $(i-1)^{\text{th}}$ bond vectors. κ quantifies the bending rigidity of the polymer.

The interaction of the polymer beads with the vertical walls are modelled by the same repulsive Lennard-Jones (rLJ) introduced before for the polymer. The surface interaction of the conical channel with the polymer is however attractive, with the attraction between the beads of the polymer and the channel beads given by the standard Lennard-Jones interaction as :

$$U_{\text{channel}}(r) = \begin{cases} 4\epsilon \left[\left(\frac{\sigma}{r}\right)^{12} - \left(\frac{\sigma}{r}\right)^6 \right], & r \leq r_c^{lj} \\ 0, & \text{otherwise} \end{cases} \quad (4)$$

where $r_c^{lj} = 2.5\sigma$.

In addition to the forces on the polymer due to its interactions with the channel, it experiences an additional external force in the positive x - direction, modeled as a potential gradient :

$$f_{\text{ext}} = \frac{f_0 d}{(d + 2x \tan \alpha)} \quad (5)$$

where f_0 is the constant force expected in a linear channel with $\alpha = 0^\circ$. Evidently, for a conical channel the force decreases along its length.

The equation of motion for the position of the i th monomer of the polymer is given by

$$m\ddot{\vec{r}}_i = -\zeta\dot{\vec{r}}_i - \nabla U_i + \vec{f}_{\text{ext}} + \vec{\eta}_i \quad (6)$$

here m is the mass of the monomer, U_i is the net potential faced by the monomer, ζ is the friction coefficient and $\vec{\eta}_i$ is a Gaussian random force with $\langle \eta_i(t)\eta_j(t') \rangle = 2k_B T \zeta \delta_{ij} \delta(t-t')$ where k_B is the Boltzmann's constant and T is the temperature. The equations are simulated in LAMMPS using the Verlet update scheme. The scales of length, energy and mass are set by σ , ϵ and m respectively. This sets the time scale as $\tau_0 = \sqrt{\frac{m\sigma^2}{\epsilon}}$. In these units, we choose $k_B T = 1.0$, $\zeta = 1.0$, $r_0 = 1.12$, $d = 1.25$ and $K = 10^3 k_B T / \sigma$. The number of polymer beads $N = 64$ and $N' = 16$ is fixed our simulations. The time step is set as $\Delta t = 0.001$ and all results presented are averaged over 1500 – 2000 independent samples.

We start our simulation by holding the first bead of the polymer at the narrow opening of the channel while the rest of the polymer segment is allowed to relax to its equilibrium conformation outside the channel. The translocation process is tracked by the translocation coordinate s . The counter for s starts once a bead of the polymer reaches the *trans* side after crossing the channel. The polymer is said to be successfully translocated if s is equal to the total number of beads N of the polymer and the simulation terminates. The speed with which the polymer traverses the channel gives a detailed idea of what is going on inside the channel. To trace the above

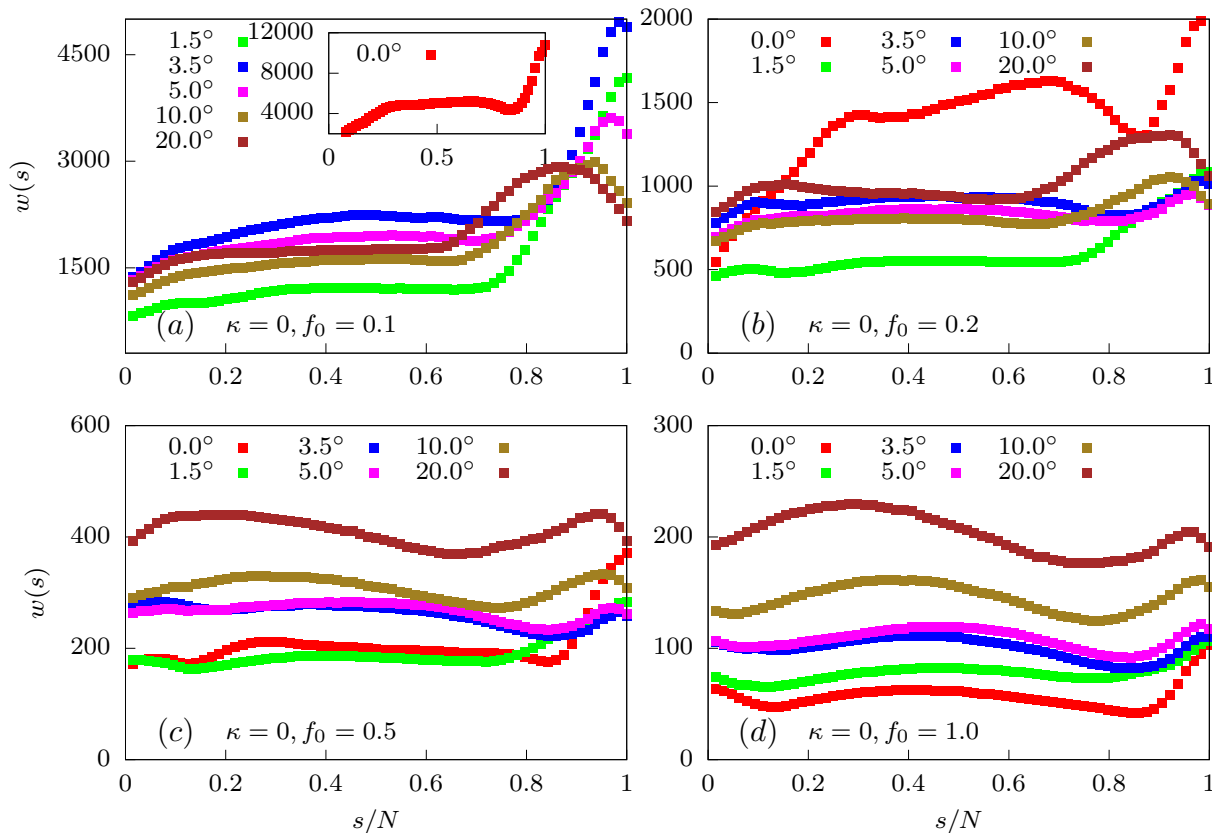


FIG. 4. Waiting time distributions of a flexible polymer for different α . In (a) we show the variation for $f_0 = 0.1$. (Inset) Plot of $w(s)$ for a flat channel which serves as a control. Increasing force values to (b) $f_0 = 0.2$, (c) $f_0 = 0.5$ and (d) $f_0 = 1.0$ leads to dramatic changes in the distribution.

effect, we focus on the waiting time $w(s)$, defined as the average time spent by a monomer inside the channel.

III. RESULTS AND DISCUSSION

A. Flexible Polymer

We first look at the translocation dynamics of a flexible polymer through a flat channel $\alpha = 0^\circ$ which serves as a control. As the strength of the external force f_0 acting inside the channel is increased ($f_{ext} = f_0$ for a flat channel), the total translocation time (τ) of the polymer decreases. At larger forces, the decrease in τ is gradual (Fig. 2(c)). To explain this behavior, we look at the waiting time distribution $w(s)$ of the polymer at different values of f_0 . Tension propagation theory [17, 19, 21, 23] accurately predicts the waiting time distribution for a slit (channel of unit size). $w(s)$ is expected to rise with s as the tension due to the external force reaches the end of the polymer in the *cis* side. After that the system is in the tail retraction stage and $w(s)$ starts decreasing with s . This broad feature is also reproduced for the

flat channel (see Fig.2(a-b)). However, there are several interesting features which arise due to the interplay between surface interactions and the external drive.

At all force values, the waiting time is high for the end monomers of the polymer. As the number of monomers left in the channel becomes lesser than the channel length and keeps decreasing, the net external force on the polymer decreases. Therefore, the attractive nature of the channel becomes a dominant factor for the end monomers resulting in increasing waiting times. For very small forces, an initial increase (as seen in slits) is observed followed by a plateau and a rise at the end monomers, as anticipated (Fig. 2(a)). At intermediate forces, the waiting time falls for the initial monomers as the higher forces favors entry into the channel. The subsequent hump at intermediate s is observed consistent with that of slits. For very large forces, this hump disappears as the entire translocation process is governed by entry and exit points (Fig. 2(b)).

We next look at the situation for $\alpha \neq 0$. As the apex angle of the channel changes, the total translocation time displays a distinct non-monotonic feature at low forces f_0 (Fig. 3). At very small channel angles, τ decreases

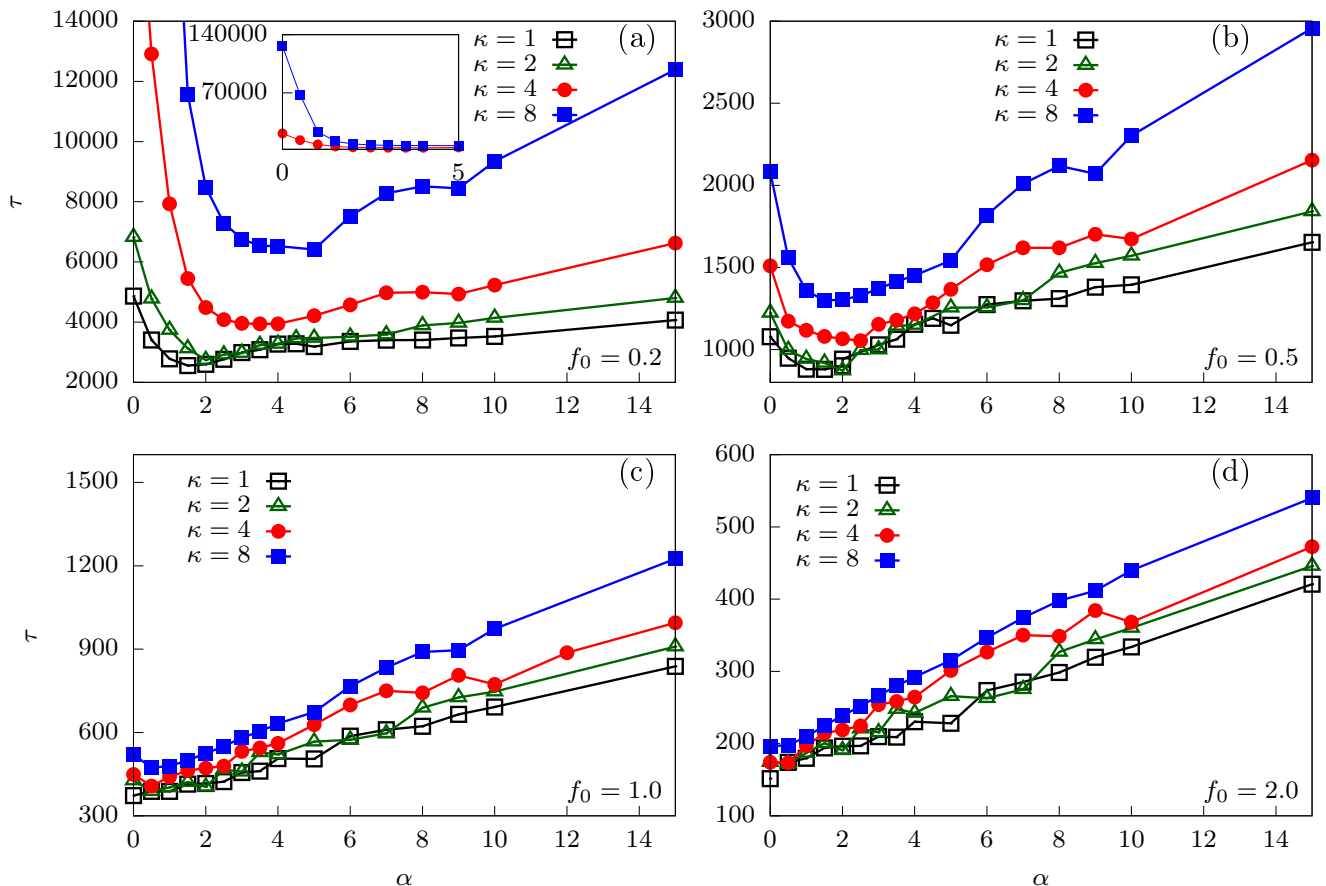


FIG. 5. Total translocation time versus α for a semiflexible polymer for four different bending rigidities $\kappa = 1, 2, 4$ and 8 . In (a) the variation is shown for $f_0 = 0.2$. (Inset) Magnified plot at lower α for $\kappa = 1.0$ and 2.0 . As external force is increased : (b) $f_0 = 0.2$ (c) $f_0 = 1.0$ and (d) $f_0 = 2.0$, τ increases almost linearly with α .

with increasing α . The entropic gain due to the larger opening facilitates translocation as compared to $\alpha = 0^\circ$, thereby reducing τ . Beyond a certain α , τ starts increasing. The effect of confinement weakens, leading to a reduction in the entropic force towards the trans side. As a result, the waiting times of even the initial monomers are larger as compared to lower α (see Fig. 4(a)).

The increase in τ with α continues till it reaches a certain α . Beyond that, τ starts to decrease with α . As α becomes large, $w(s)$ for the end monomers shows a dip rather than monotonically rising as observed for smaller α . The surface interactions becomes substantially weaker for the end monomers. Although the entropic force which reduced translocation times for smaller angles is now weaker, the polymer segment inside the channel near the trans end can now coil, with hairpin formations becoming more and more prevalent. The interaction with the wall is no longer the limiting process, although it still resists translocation. Therefore, exiting the channel becomes progressively easier.

With increasing f_0 , we see a curious behaviour. At higher forces, τ is seen to effectively increase with α . This is also reflected in the waiting time distributions

(see Fig. 4(c-d)). To understand this behavior, note that for higher forces, the surface interactions do not play a major role. The force along the channel axis is larger for smaller α . This ensures that at large force values the translocation process is extremely fast. As α increases, the force along the channel axis decreases and translocation becomes slower.

B. Semiflexible Polymer

We now discuss the translocation dynamics of a driven semiflexible polymer through the conical channel. We first look at the total translocation time as function of the apex angle for different values of polymer rigidity and external driving force. In Fig. 5(a), we have plotted τ as function of α for a low external force value ($f_0 = 0.2$). The variation of the translocation time with apex angle still shows a non-monotonic feature as observed in the case of a flexible polymer. However, unlike that of the flexible polymer, rigid polymers do not show a sharp secondary peak in τ . The total translocation time shows an initial decrease with increasing α indicating that as the

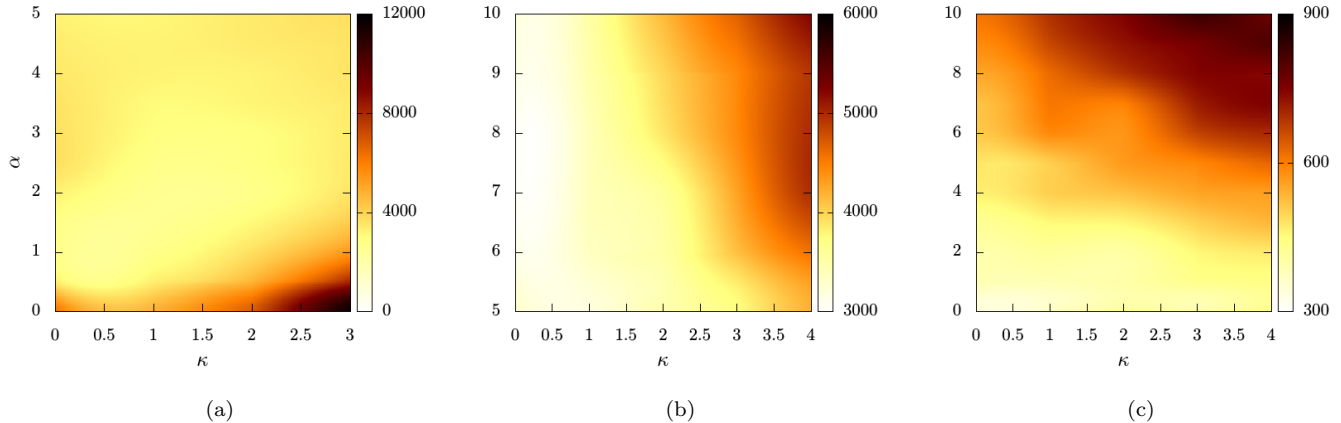


FIG. 6. Phase plot of total translocation time τ in the $\kappa - \alpha$ plane. In (a) and (b) we have shown the phase plot at $f_0 = 0.2$ for two different ranges of α : $[0^\circ, 5^\circ]$ and $[5^\circ, 10^\circ]$. (c) Phase plot for $f_0 = 1.0$.

apex angle increases, it becomes favorable for the polymer to exit the channel. However, beyond a critical α , translocation time starts increasing monotonically with α . This increase in τ with increasing α is drastically different from that of the flexible polymer. Further, with increasing rigidity of the polymer the translocation time increases for all values of α . This feature is consistent with earlier results of driven translocation of semiflexible polymers through extended channels [39, 57]. Also note that the critical α shifts to larger values of apex angle as the rigidity of the polymer is increased.

As the external force is increased, the non-monotonicity observed in the variation of τ with α starts decreasing. In Figs. 5(b-d), we observe that at higher force values, the critical α keeps shifting to lower values of the apex angle. At very high forces, the total translocation time increases monotonically with the apex angle for all rigidities of the polymer. In Fig. 6 we construct phase plots for τ in the $\kappa - \alpha$ plane for various values of f_0 . Fig. 6(a) indicates that τ is maximum for stiffer chains and at smaller apex angles for small forces. For the same force value we have a phase plot for larger α in Fig. 6(b). The phase plot shows a dramatic change with larger translocation times now observed for higher apex angles (Fig. 6(b)). At even larger forces, the phase plot shows a largely uniform increase in τ with increasing α for all κ values (Fig. 6(c)).

To better understand the dynamics, we look at the waiting time distributions of the semiflexible polymer as it moves from the *cis* to the *trans* side of the channel at low forces. In Fig. 7, we have plotted $w(s)$ for different values of the bending rigidity as the apex angle is varied. For low bending rigidity, $w(s)$ shows an increase with s initially and then a largely flat region at intermediate s , for all values of α (Fig. 7(a)). These results are consistent with that obtained for uniformly extended channels. However, near $s \approx N$, there is a great variation in $w(s)$

for different α values. For smaller values of α , $w(s)$ shows a sharp rise near $s = N$. This can be attributed to the attractive nature of the surface interactions which prohibits escape of the end monomers to the *trans* side. With increasing apex angle, the monomers exiting the channel do not feel the interactions as strongly as before. As a result $w(s)$ shows a dip near $s = N$ for large α . Further we note that the entire waiting time distribution falls initially for small apex angles (from $\alpha = 0^\circ$ to $\alpha = 1.5^\circ$ in Fig. 7(a)) and then increases monotonically with increasing α mimicking the behavior of τ as expected.

With increasing bending rigidity (Fig. 7(b-d)), there is an overall increase in the waiting time of all monomers. For the end monomers exiting the channel, this increase is especially sharp. With stiffer chains, translocation becomes progressively difficult. This is consistent with earlier observations of translocation of semiflexible polymers. As the polymer rigidity increases, the entropic gain in moving towards the *trans* end of the conical channel becomes lesser. The translocation dynamics of the end monomers is now dominated by the attractive surface interactions. The end segment of the polymer keeps deflecting between the walls and are stuck in either wall for long periods, thereby increasing the waiting times. It is interesting to note that even at high κ , the non-monotonic behavior in $w(s)$ with α persists.

IV. FREE ENERGY

It has been established that the relaxation time of a polyelectrolyte chain in equilibrium is much shorter than the translocation time for the typical range of chain lengths used and typical voltages applied in most experiments [31]. This implies that a polymer chain initially at equilibrium can be taken to be in quasi-equilibrium as it translocates across the nanochannel especially for low ex-

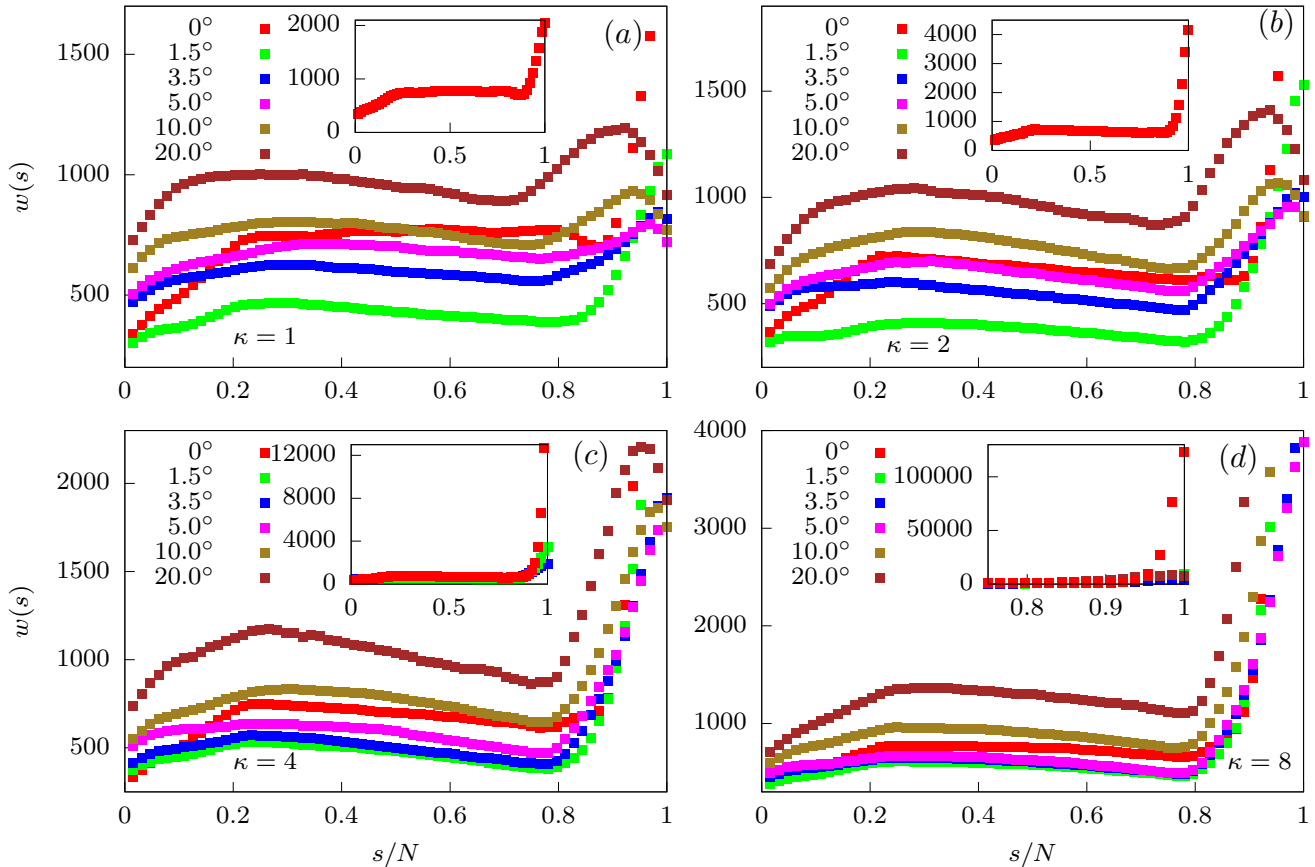


FIG. 7. Waiting time distributions for various α at (a) $\kappa = 1$, (b) $\kappa = 2$, (c) $\kappa = 4$ and (d) $\kappa = 8$. The distributions show dramatic changes as the bending rigidity of the polymer is increased. (Insets) Plots of the distribution at the various κ values for a flat channel.

ternal forces. In fact the quasi-equilibrium approximation in such cases can be even extended to translocation of every segment of the polymer [31]. The quasi-equilibrium approximation obviously fails for high forces and longer lengths of the polymer. Using this approximation for low forces and chain lengths considered in our simulations, we construct the free energy landscape for the translocation process to understand the translocation behavior obtained in our simulations.

There are several contributions to the free energy : (i) the entropic contribution coming from the confinement of the polymer segment inside the channel (ii) entropic contribution due to the polymer segments outside the channel (ii) energetic contribution due to surface interactions between the channel and the polymer and (iv) energetic contribution due to the external force. The total free energy of the system in terms of the translocation coordinate can be written as

$$\mathcal{F}_t(s) = \mathcal{F}_e + \mathcal{F}_c + \mathcal{F}_{pp} \quad (7)$$

where \mathcal{F}_c is the confinement free energy, \mathcal{F}_e is the entropic component due to polymer segments outside the channel and \mathcal{F}_{pp} is the free energy contribution due to

the channel polymer interactions.

To construct \mathcal{F}_e for a semiflexible polymer segment inside a conical channel, we use the approach in [53]. The contribution to the free-energy from a polymer of size R confined in an area A of the cone in two dimensions is given as $\mathcal{F}_c \sim k_B T \left(\frac{R^2}{A} \right)^{\frac{1}{2\nu-1}}$ [58]. If N_p denotes the number of polymer beads confined inside the channel, then $R \sim \sigma N_p^\nu$, where $\nu = 3/4$ is the Flory exponent in two dimensions. A is dependent on the degree of confinement. If L denotes the length of the region inside the channel along the x -direction that holds the confined polymer and a the length which is empty, then A is given as $A = \frac{1}{4 \tan \alpha} [(D_0 + 2(a+L) \tan \alpha)^2 - (D_0 + 2a \tan \alpha)^2]$.

In the case of rigid polymers, the analysis can be extended by replacing the number of monomers N_p with the number of Kuhn segments $\tilde{N}_p \approx N_p \sigma / l_K$ where $l_K = 2l_p$ is the Kuhn length. l_p is the persistence length of the polymer. In two dimensions, the bending rigidity is related to the persistence length as $\kappa / k_B T = l_p / 2$. We would however like to express \mathcal{F}_e in terms of the translocation coordinate s . Therefore, we extract the number

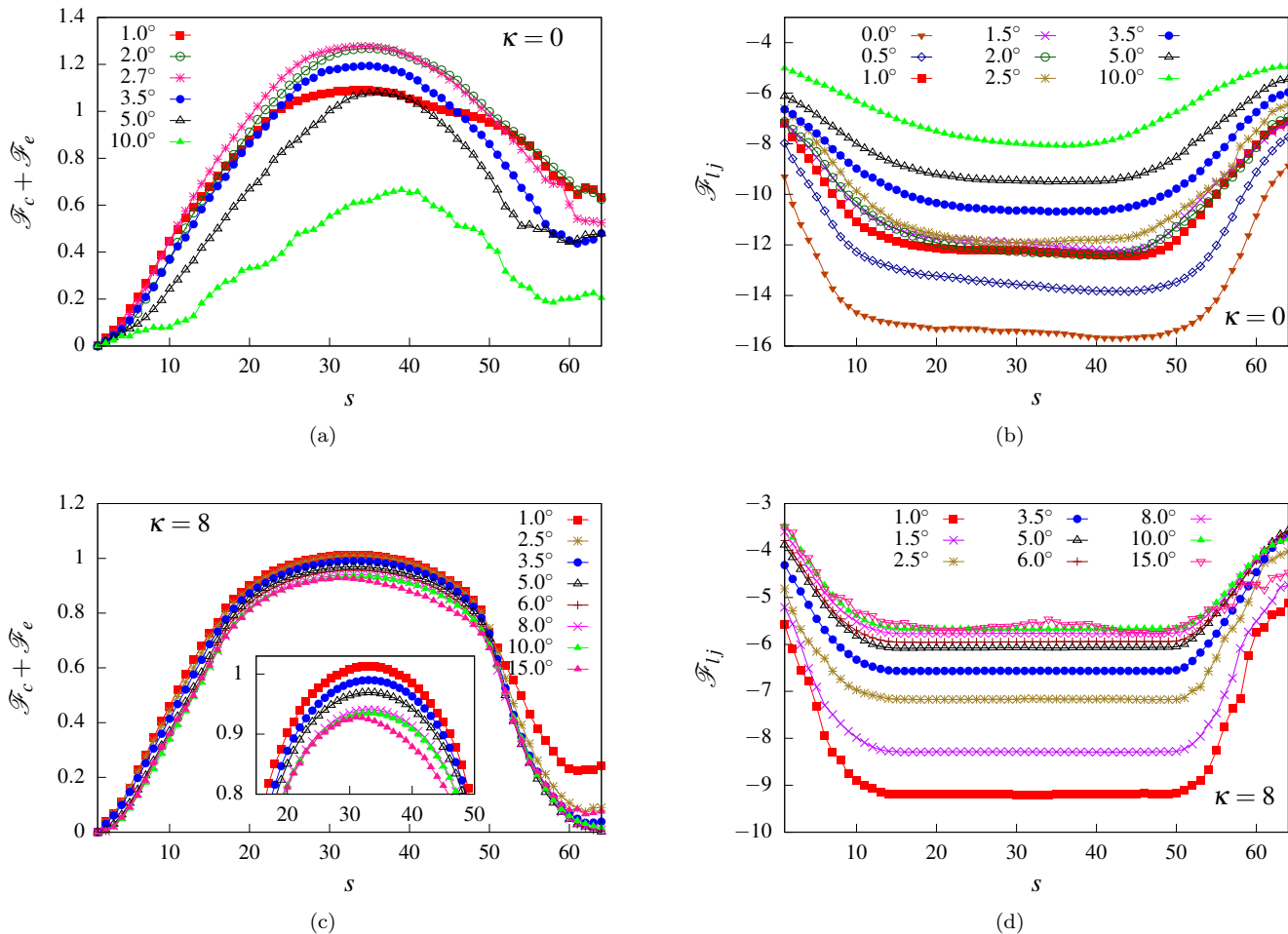


FIG. 8. (a) Entropic part of the free energy ($\mathcal{F}_c + \mathcal{F}_e$) for a flexible polymer as a function of the translocation coordinate s for different α values showing non-monotonic behavior. (b) Energetic contribution to free energy for a flexible polymer from surface interactions (\mathcal{F}_{lj}) as a function of translocation coordinate s for various α values. (c) Entropic part of the free energy ($\mathcal{F}_c + \mathcal{F}_e$) for a semiflexible polymer ($\kappa = 8$) as a function of the translocation coordinate s for different α values showing largely monotonic behavior. (Inset) The barrier height decreases monotonically with α . (d) Energetic contribution to free energy for the semiflexible polymer from surface interactions (\mathcal{F}_{lj}) as a function of translocation coordinate s for various α values.

of beads that are inside the channel from the simulations for a fixed translocation coordinate. As is expected, there would be several configurations of the polymer (with different values of N_p) inside the channel for a given s . The confinement free energies of all such configurations are averaged to give $\mathcal{F}_c(s)$.

The free energy contribution from the polymer segments outside the channel is given as[26]:

$$\mathcal{F}_e = \begin{cases} \gamma' \log N_c & N_c > 1 \text{ and } N_t = 0 \\ \gamma' \log N_c + \gamma' \log N_t & N_c > 1 \text{ and } N_t > 1 \\ \gamma' \log N_t & N_c = 0 \text{ and } N_t > 1 \end{cases}$$

where N_c is the number of beads on the cis-side of the channel and N_t is the number of beads on the trans-side of the channel. Note that N_c , N_t are functions of the translocation coordinate s and are obtained from the

simulation similar to the confinement free energy for every value of s . Further, $N_c + N_p + N_t = N$ at all times.

The free energy contribution from the surface interaction \mathcal{F}_{lj} is obtained by summing over the LJ potential felt by each polymer bead when they are inside the channel. For a given translocation coordinate, we identify the number of beads inside the channel and calculate the total potential felt by the beads. As we mentioned before, for a given s , there would be multiple configurations of the polymer inside the channel (corresponding to the time steps for which $s = 1, 2, \dots$). All such contributions are appropriately accounted for and the averaged free energy contribution \mathcal{F}_{lj} due to surface interactions is evaluated numerically as the translocation coordinate changes.

In Fig. 8(a), we plot the total free energy contributions which are entropic in origin for a flexible polymer,

arising due to the confined segments of the polymer and the segments outside the channel. The free energy contribution due to channel-polymer interactions are plotted in Fig. 8(b). The entropic contribution exhibits a free energy barrier for an intermediate s for all values of the channel angle α . This indicates that entropically it is more difficult for the polymer to enter the channel from the cis side. However, the energetic contribution coming from the attractive LJ potential dominates the initial stages and the polymer is sucked into the channel. At intermediate s , the competition between the two leads to the comparatively larger waiting times observed in Fig. 4. As α is increased, we observe a clear non-monotonic behavior in the entropic part of the free energy. The free energy barrier increases as we go from $\alpha = 1.0^\circ$ to $\alpha = 2.7^\circ$ and decreases as α is increased further. This indicates that translocation would be more difficult from $\alpha = 1.0^\circ$ to $\alpha = 2.7^\circ$ and favorable as the channel angle increases. This is consistent with the behavior observed in the translocation time as a function of the channel angle, where for $f_0 = 0.1$, τ shows a peak at $\alpha \approx 2.7^\circ$ and decreases with increasing α . The energetic contribution \mathcal{F}_{lj} does not show non-monotonic behavior at these values of α , with significant overlap in the free energy profiles (see Fig. 8(b)). As α is increased, \mathcal{F}_{lj} becomes shallower indicating easier translocation and therefore decreasing τ .

In Fig. 8(c), we plot the total free energy contributions which are entropic in origin for a semiflexible polymer for various channel angles. Similar to the flexible polymer, the entropic contribution indicates a barrier at intermediate s . However, unlike the flexible polymer, this barrier reduces monotonically with increasing α . The corresponding free energy contribution due to channel-polymer interactions also becomes shallower monotonically as α is increased (see Fig. 8(d)). Therefore, for a semiflexible polymer, translocation becomes easier with increasing α . If we compare our analytical predictions with that of the simulation results in Fig. 5(a) for $\kappa = 8$, we find that translocation time indeed decreases with increasing α upto $\alpha = 6^\circ$ consistent with our predictions. However, for larger channel angles, the translocation time increases. This behavior is very different from the predictions from the free energy calculations.

In order to understand this behavior, it is crucial to look at the potential landscape inside the channel. At large channel angles, the strength of the potential due to the channel walls becomes negligible for large regions inside the channel. Even during entry of the polymer from the cis side of the channel, the attractive potential becomes much weaker in the region close to the cis side for large angles. This hampers the pulling ability of the channel resulting in larger waiting times of even the initial beads of the polymer. As the polymer is pulled in, the segments of the stiff polymer inside the channel keeps getting deflected from one wall to the other (see Supplementary Movie). The potential near the centre of the channel is negligible as is the external force and the

polymer segments stay attached to either wall for considerable times. This leads to increasing translocation times at higher channel angles. For smaller channel angles, the average positions of the polymer segments are much closer to the middle of the channel as both walls try to pull on them. With external force much stronger near the center, the polymer is pulled out faster. Note that for flexible polymers, the possibility of more conformations of the polymer as compared to stiffer chains at larger angles ensures that the situation is much more homogeneous and we do not observe much change at larger channel angles.

V. DISCUSSIONS

The translocation of polymers through asymmetric shaped channels has sparked a lot of interest due to its significant advantages in bio-sensing applications. Buoyed by experimental studies using conical nanochannels, we have studied the translocation dynamics of a semiflexible polymer through such a channel under the influence of a spatially varying external drive and attractive surface interactions. The waiting time distribution show rich features arising due to the polymer stiffness, surface interactions and nature of the external drive. We attempt to understand some of these features using a free energy argument based on a quasi-equilibrium approximation which is applicable for smaller polymer lengths and low forces. The theory captures some of the non-monotonic features of the translocation dynamics. At higher stiffness and larger channel angles, the variable potential landscape arising from the surface interactions becomes dominant. This variability needs to be accounted for in order to provide a more accurate description of the dynamics.

Recent experiments have revealed that driven polymer translocation through synthetic nanopores is a two stage process with translocation initially slowing with time before accelerating close to the end of the process [52]. In our detailed simulations, we show however that the translocation dynamics is strongly dependent on the stiffness of the polymer and surface interactions. Attractive surface interactions can considerably slow down the translocation process near the ends while increasing the angle of the conical pore may facilitate the process. We have considered one possible conical structure where the polymer enters the pore from the constricted side of the channel. In future work we will explore the detailed dynamics of the polymer as it enters from the wider end of the channel which is expected to give rise to significantly different dynamics due to the asymmetry of the channel.

VI. ACKNOWLEDGEMENTS:

AS acknowledges University Grants Commission (UGC), India for the financial support under the UGC-

JRF/SRF scheme. We are thankful to the computational facility provided by IISER, Mohali.

-
- [1] M. Muthukumar, *Polymer translocation* (CRC press, 2016).
- [2] V. V. Palyulin, T. Ala-Nissila, and R. Metzler, *Soft matter* **10**, 9016 (2014).
- [3] D. Branton, D. W. Deamer, A. Marziali, H. Bayley, S. A. Benner, T. Butler, M. Di Ventra, S. Garaj, A. Hibbs, X. Huang, *et al.*, in *Nanoscience and technology: A collection of reviews from Nature Journals* (World Scientific, 2010) pp. 261–268.
- [4] M. Wanunu, *Physics of life reviews* **9**, 125 (2012).
- [5] S. Howorka and Z. Siwy, *Chemical Society Reviews* **38**, 2360 (2009).
- [6] U. F. Keyser, *Journal of The Royal Society Interface* **8**, 1369 (2011).
- [7] A. Milchev, *Journal of Physics: Condensed Matter* **23**, 103101 (2011).
- [8] S. M. Bezrukov, I. Vodyanoy, and V. A. Parsegian, *Nature* **370**, 279 (1994).
- [9] J. J. Kasianowicz, E. Brandin, D. Branton, and D. W. Deamer, *Proceedings of the National Academy of Sciences* **93**, 13770 (1996).
- [10] W. Sung and P. Park, *Physical review letters* **77**, 783 (1996).
- [11] P. J. Park and W. Sung, *The Journal of chemical physics* **108**, 3013 (1998).
- [12] M. Muthukumar, *The Journal of Chemical Physics* **111**, 10371 (1999).
- [13] M. Muthukumar, *The Journal of chemical physics* **118**, 5174 (2003).
- [14] T. Sakaue, *Physical Review E* **76**, 021803 (2007).
- [15] T. Sakaue, *Physical Review E* **81**, 041808 (2010).
- [16] T. Saito and T. Sakaue, *Physical Review E* **85**, 061803 (2012).
- [17] J. Sarabadani, T. Ikonen, and T. Ala-Nissila, *The Journal of Chemical Physics* **141**, 214907 (2014).
- [18] P. Rowghanian and A. Y. Grosberg, *The Journal of Physical Chemistry B* **115**, 14127 (2011).
- [19] T. Ikonen, A. Bhattacharya, T. Ala-Nissila, and W. Sung, *Physical Review E* **85**, 051803 (2012).
- [20] T. Ikonen, A. Bhattacharya, T. Ala-Nissila, and W. Sung, *EPL (Europhysics Letters)* **103**, 38001 (2013).
- [21] T. Ikonen, A. Bhattacharya, T. Ala-Nissila, and W. Sung, *The Journal of chemical physics* **137**, 085101 (2012).
- [22] A. Bhattacharya and K. Binder, *Physical Review E* **81**, 041804 (2010).
- [23] A. Bhattacharya, *Polymer Science Series C* **55**, 60 (2013).
- [24] H. W. de Haan and G. W. Slater, *Physical Review E* **81**, 051802 (2010).
- [25] M. G. Gauthier and G. W. Slater, *The Journal of chemical physics* **128**, 02B612 (2008).
- [26] M. G. Gauthier and G. W. Slater, *The Journal of Chemical Physics* **128**, 05B619 (2008).
- [27] A. Huang, A. Bhattacharya, and K. Binder, *The Journal of Chemical Physics* **140**, 214902 (2014).
- [28] K. Luo, T. Ala-Nissila, S.-C. Ying, and A. Bhattacharya, *Physical Review Letters* **99**, 148102 (2007).
- [29] J. Sarabadani and T. Ala-Nissila, *Journal of Physics: Condensed Matter* **30**, 274002 (2018).
- [30] P. M. Suhonen and R. P. Linna, *Physical Review E* **97**, 062413 (2018).
- [31] H. H. Katkar and M. Muthukumar, *The Journal of chemical physics* **148**, 024903 (2018).
- [32] G. F. Schneider and C. Dekker, *Nature biotechnology* **30**, 326 (2012).
- [33] L.-Z. Sun and M.-B. Luo, *Journal of Physics: Condensed Matter* **26**, 415101 (2014).
- [34] L.-Z. Sun, H. Li, X. Xu, and M.-B. Luo, *Journal of Physics: Condensed Matter* **30**, 495101 (2018).
- [35] C. T. A. Wong and M. Muthukumar, *The Journal of chemical physics* **133**, 07B607 (2010).
- [36] A. Meller, L. Nivon, and D. Branton, *Physical Review Letters* **86**, 3435 (2001).
- [37] A. Meller, *Journal of physics: condensed matter* **15**, R581 (2003).
- [38] J. A. Cohen, A. Chaudhuri, and R. Golestanian, *Physical Review X* **2**, 021002 (2012).
- [39] R. Kumar, A. Chaudhuri, and R. Kapri, *The Journal of chemical physics* **148**, 164901 (2018).
- [40] I. M. Derrington, T. Z. Butler, M. D. Collins, E. Manrao, M. Pavlenok, M. Niederweis, and J. H. Gundlach, *Proceedings of the National Academy of Sciences* **107**, 16060 (2010).
- [41] B. M. Venkatesan and R. Bashir, *Nature nanotechnology* **6**, 615 (2011).
- [42] C. Dekker, *Nanoscience And Technology: A Collection of Reviews from Nature Journals*, 60 (2010).
- [43] M. Wanunu and A. Meller, *Nano letters* **7**, 1580 (2007).
- [44] M. Gershow and J. A. Golovchenko, *Nature nanotechnology* **2**, 775 (2007).
- [45] B. Luan, G. Stolovitzky, and G. Martyna, *Nanoscale* **4**, 1068 (2012).
- [46] U. F. Keyser, B. N. Koeleman, S. Van Dorp, D. Krapf, R. M. Smeets, S. G. Lemay, N. H. Dekker, and C. Dekker, *Nature Physics* **2**, 473 (2006).
- [47] J. Mathé, A. Aksimentiev, D. R. Nelson, K. Schulten, and A. Meller, *Proceedings of the National Academy of Sciences* **102**, 12377 (2005).
- [48] C. C. Harrell, Y. Choi, L. P. Horne, L. A. Baker, Z. S. Siwy, and C. R. Martin, *Langmuir* **22**, 10837 (2006).
- [49] W.-J. Lan, D. A. Holden, and H. S. White, *Journal of the American Chemical Society* **133**, 13300 (2011).
- [50] V. V. Thacker, S. Ghosal, S. Hernández-Ainsa, N. A. Bell, and U. F. Keyser, *Applied physics letters* **101**, 223704 (2012).
- [51] J. Zhou, Y. Wang, L. D. Menard, S. Panyukov, M. Rubinstein, and J. M. Ramsey, *Nature communications* **8**, 1 (2017).
- [52] K. Chen, I. Jou, N. Ermann, M. Muthukumar, U. F. Keyser, and N. A. Bell, *Nature Physics* **17**, 1043 (2021).
- [53] N. Nikoofard, H. Khalilian, and H. Fazli, *The Journal of Chemical Physics* **139**, 074901 (2013).
- [54] N. Nikoofard and H. Fazli, *Soft Matter* **11**, 4879 (2015).
- [55] B. Tu, S. Bai, B. Lu, and Q. Fang, *Scientific reports* **8**, 1 (2018).

- [56] L.-Z. Sun, W.-P. Cao, C.-H. Wang, and X. Xu, *The Journal of Chemical Physics* **154**, 054903 (2021).
- [57] R. Adhikari and A. Bhattacharya, *The Journal of Chemical Physics* **138**, 204909 (2013).
- [58] T. Sakaue and E. Raphaël, *Macromolecules* **39**, 2621 (2006).